The Astrophysical Journal, 862:137 (11pp), 2018 August 1 https://doi.org/10.3847/1538-4357/aacaf7

The Quest for the Inflationary Spectral Runnings in the Presence of Systematic Errors

Xiaolei Li[1,2], Noah Weaverdyck[2], Saroj Adhikari[2], Dragan Huterer[2], Jessica Muir[2], and Hao-Yi Wu[3]
[1] Department of Astronomy, Beijing Normal University, Beijing, 100875, People's Republic of China; lixiaolei@mail.bnu.edu.cn
[2] Department of Physics, University of Michigan, 450 Church Street, Ann Arbor, MI 48109-1040, USA
[3] Center for Cosmology and Astro-Particle Physics, The Ohio State University, Columbus, OH 43210-1117, USA
Received 2018 March 16; revised 2018 May 17; accepted 2018 June 4; published 2018 July 31

Abstract

Cosmological inflation predicts that the scalar spectral index "runs" with scale. Constraints on the values of the spectral runnings, $\alpha_s \equiv dn_s/d\ln k$ and $\beta_s \equiv d\alpha_s/d\ln k$, therefore provide a fundamental test of the physics of inflation. Here, we study the feasibility of measuring the runnings when information from upcoming large-volume galaxy surveys is used to supplement the information provided by a cosmic microwave background (CMB)-S4 experiment, particularly focusing on the effect of including high-k, nonlinear scales. Since these measurements will be sensitive to modeling uncertainties for the nonlinear power spectrum, we examine how three different ways of parameterizing those systematics—introducing zero, two, or several hundred nuisance parameters—affect constraints and protect against parameter biases. Considering statistical errors alone, we find that including strongly nonlinear scales can substantially tighten constraints. However, these constraints weaken to levels not much better than those from a CMB-S4 experiment alone when we limit our analysis to scales where estimates are not strongly affected by systematic biases. Given these considerations, near-future large-scale structure (LSS) surveys are unlikely to add much information to the CMB-S4 measurement of the first running α_s. There is more potential for improvement for the second running, β_s, for which LSS information will allow constraints to be improved by a factor of 3–4 relative to using the CMB alone. Though these constraints are still above the value predicted by slow-roll inflation, they do probe regions of parameter space relevant to nonstandard inflationary models with large runnings, for example, those that can generate an appreciable abundance of primordial black holes.

Key words: cosmological parameters – inflation – large-scale structure of universe – methods: statistical

1. Introduction

Cosmological inflation (Guth 1981; Albrecht & Steinhardt 1982; Linde 1982) has passed observational tests with flying colors: the combination of the cosmic microwave background (CMB) with measurements of large-scale structure (LSS) confirms that the geometry of the universe is nearly flat and that the spectrum of density fluctuations is almost scale invariant (Bardeen et al. 1983). The super-horizon fluctuations observed in the temperature-polarization cross-correlation in the CMB behave in precisely the way that inflation predicts (Dodelson 2003). Beyond these successes, the most important upcoming test of inflation is the search for the signature of primordial gravitational waves, which inflation generically predicts, in the CMB polarization. In this paper, we study the prospects of another important test of inflation: the search for the running of the scalar spectral index.

The primordial power spectrum of curvature fluctuations can be parameterized by Taylor expanding about a pivot scale k_*

$$\frac{k^3}{2\pi^2}P_s(k) = A_s\left(\frac{k}{k_*}\right)^{(n_s-1)+\frac{1}{2}\alpha_s\ln(k/k_*)+\frac{1}{6}\beta_s(\ln(k/k_*))^2+\ldots}, \quad (1)$$

where A_s is the scalar amplitude, n_s is the spectral index, and α_s and β_s are its first and second derivatives, respectively, evaluated at the pivot scale k_*. Single-field slow-roll inflation models predict the power spectrum to be nearly scale invariant, i.e., $n_s \approx 1$, a prediction borne out through measurements of the CMB. The *Planck* experiment (Ade et al. 2016a) has constrained these parameters for the ΛCDM+α_s model, measuring $n_s = 0.968 \pm 0.006$ and $\alpha_s = -0.003 \pm 0.007$ at the pivot $k_* = 0.05\,\mathrm{Mpc}^{-1}$. Expanded to include the second running, the *Planck* constraints become $n_s = 0.959 \pm 0.006$, $\alpha_s = 0.009 \pm 0.010$, and $\beta_s = 0.025 \pm 0.013$ (see also Cabass et al. 2016).

In single-field slow-roll inflationary models, the runnings are of the order of $\alpha_s \sim (1-n_s)^2 \sim 10^{-3}$ and $\beta_s \sim (1-n_s)^3 \sim 4\times10^{-5}$ (Kosowsky & Turner 1995; see also Garcia-Bellido & Roest 2014; Escudero et al. 2016), levels far below the sensitivity of the *Planck* satellite mission, but potentially reachable with new generations of CMB and LSS surveys. Detection of the runnings with magnitudes larger than these values would indicate that the mechanism that generated the primordial fluctuations cannot just be described by a single-field slow-roll model (Easther & Peiris 2006; Vieira et al. 2018). It is possible, for example, for large runnings to be generated by modulations to the inflationary potential (Kobayashi & Takahashi 2011; Czerny et al. 2014). It has also been proposed that modulations resulting in a large value of $\beta_s \sim 10^{-3}$ could produce an appreciable number of primordial black holes (PBHs; Drees & Erfani 2012); at $\beta_s \approx 0.03$, these PBHs would be large enough to be a dark matter candidate (Carr et al. 2016; Muñoz et al. 2017). Thus, even bounds on inflationary spectral runnings that are above the level needed to test single-field slow-roll inflation can provide valuable information.

Muñoz et al. (2017) investigated how well future surveys will be able to measure α_s and β_s, using a CMB Stage 4 (CMB-S4) experiment in combination with various LSS surveys. They find that even with the combination of a billion-object survey such as SKA, the runnings will only be measured to $\sigma_\alpha = 9.3\times10^{-4}$ and $\sigma_\beta = 2\times10^{-3}$, which are levels that are insufficient for a significant detection if the values are near those predicted by single-field slow-roll inflation (see Huang

et al. 2012; Amendola et al. 2013; Basse et al. 2015 for other forecasts on spectral runnings constraints using CMB and future LSS surveys). It is worth noting, however, that these forecasts only make use of LSS data that are comfortably within the linear regime ($k \lesssim 0.1\,h\,\mathrm{Mpc}^{-1}$). LSS surveys measure tracers of the matter power spectrum $P_m(k, z)$, and in principle can access information deep in the nonlinear regime, up to $k \simeq 1\,h\,\mathrm{Mpc}^{-1}$ and beyond. The combination of large scales accessed by the CMB and small scales accessed by the LSS is particularly important for constraining the spectral index and its running, as the long lever arm in wavenumber helps to break degeneracies with other cosmological parameters.

Using information from small scales (large k) introduces significant challenges, however. Fluctuations in matter density become large at small scales, so at some scale linear perturbation theory becomes insufficient to describe their evolution. There is a significant ongoing effort to improve our understanding of structure growth in this nonlinear regime (Bernardeau et al. 2002; Smith et al. 2003; Heitmann et al. 2009, 2010; Lawrence et al. 2010). Baryonic effects also become important at these scales and affect the power spectrum of LSS tracers (Rudd et al. 2008; van Daalen et al. 2011; Chisari et al. 2018). In addition, nonlinearities at small scales induce correlations between wavenumbers (Scoccimarro et al. 1999), so that the covariance of power spectra evaluated at two wavenumbers depends on the nontrivial matter trispectrum.

It is therefore of fundamental importance to understand to what extent the small-scale systematics in the LSS can be parameterized and self-calibrated in order to utilize those scales in the search for α_s and β_s. The main goal of this paper is to assess how constraints on the runnings improve as LSS information at higher wavenumbers is added to the analysis. We investigate how the results are biased when the nonlinear regime is mismodeled, and how well this bias can be mitigated through the inclusion of nuisance parameters at small scales.

The paper is organized as follows. In Section 2, we describe our methodology in detail: our fiducial cosmological model, the CMB and LSS surveys considered, and the Fisher matrix formalism we use for forecasting constraints. In Section 3, we present and discuss our forecast for the spectral running α_s constraints using future galaxy surveys alone and in combination with CMB-S4. We then introduce the Fisher bias formalism for modeling systematic bias in cosmological parameters, and discuss the corresponding results for α_s in Section 4. In Section 5, we present our constraints and systematic bias results for the second spectral running, β_s. We summarize our findings and conclude in Section 6.

2. Methods

In this section, we describe our fiducial model for CMB and LSS observations and describe our forecasting methodology, which makes use of the Fisher matrix formalism to forecast the precision of measurements of the runnings.

2.1. Fiducial Model

We assume a flat ΛCDM cosmology with six parameters in addition to the spectral runnings: the physical baryon and CDM densities $\Omega_b h^2$ and $\Omega_c h^2$, the reionization optical depth τ, the Hubble constant H_0, the scalar spectral index n_s, and the primordial power spectrum amplitude A_s. The values of these parameters in our fiducial model are listed in Table 1.

Table 1
Cosmological Parameters, Their Fiducial Values, and Numerical Derivative Step Sizes Used for the Fisher Matrix Calculation

Parameter (p_i)	Fiducial Value	Step Size (Δp_i)
$\Omega_b h^2$	0.02222	±1%
$\Omega_c h^2$	0.1197	±1%
τ	0.06	±1%
H_0	67.5	±1%
n_s	0.9655	±1%
$10^{10} A_s$	21.96	±1%
α_s	0	$\pm 1 \times 10^{-3}$
β_s	0	$\pm 1 \times 10^{-3}$
A_{bary}	3.13	±5%
η_0	0.6044	±5%

Note. The last two parameters correspond to the Mead model for describing nonlinear effects.

2.2. Modeling the CMB

The CMB fluctuations have a wealth of information about the early universe, providing some of the tightest constraints for cosmology to date (Ade et al. 2016b). The observed CMB angular power spectrum can be related to the primordial power spectrum $P_s(k)$ that sourced those fluctuations via

$$C_\ell^{XY} = \frac{2}{\pi} \int dk\, k^2 P_s(k) \Delta_\ell^X(k) \Delta_\ell^Y(k). \tag{2}$$

Labels X and Y can refer to temperature (T), polarization modes (E, B), or lensing potential (d), and Δ_ℓ^X is the transfer function that encompasses both source and projection terms integrated over the line of sight.

Taking T and E as our observables, the observed angular power spectra can be represented as a vector $(C_\ell^{TT}, C_\ell^{EE}, C_\ell^{TE})$ with covariance matrix

$$\mathrm{Cov}_\ell = \frac{2}{(2\ell+1) f_{\mathrm{sky}}} \times \begin{pmatrix} (\tilde{C}_\ell^{TT})^2 & (\tilde{C}_\ell^{TE})^2 & \tilde{C}_\ell^{TT}\tilde{C}_\ell^{TE} \\ (\tilde{C}_\ell^{TE})^2 & (\tilde{C}_\ell^{EE})^2 & \tilde{C}_\ell^{EE}\tilde{C}_\ell^{TE} \\ \tilde{C}_\ell^{TT}\tilde{C}_\ell^{TE} & \tilde{C}_\ell^{EE}\tilde{C}_\ell^{TE} & \frac{1}{2}[(\tilde{C}_\ell^{TE})^2 + \tilde{C}_\ell^{TT}\tilde{C}_\ell^{EE}] \end{pmatrix} \tag{3}$$

where the auto power spectra include contributions from noise:

$$\begin{aligned} \tilde{C}_\ell^{TT} &= C_\ell^{TT} + N_\ell^{TT} \\ \tilde{C}_\ell^{EE} &= C_\ell^{EE} + N_\ell^{EE} \\ \tilde{C}_\ell^{TE} &= C_\ell^{TE}. \end{aligned} \tag{4}$$

We adopt the same noise properties for a CMB-S4 experiment used by Muñoz et al. (2017):

$$N_\ell^{TT} = \Delta_T^2 \exp\left[\frac{\ell(\ell+1)\theta_{\mathrm{FWHM}}^2}{8 \ln 2}\right] \tag{5}$$

and

$$N_\ell^{EE} = 2 \times N_\ell^{TT}, \tag{6}$$

where the temperature sensitivity is $\Delta_T = 1\,\mu$K arcmin and the beam full-width-half-maximum is $\theta_{\mathrm{FWHM}} = 8.7 \times 10^{-4}$ radians (Abazajian et al. 2016). We assume a sky coverage of $f_{\mathrm{sky}} = 0.4$

and that the usable range of multipoles is $\ell \in [30, 3000]$ for C_ℓ^{TT} and C_ℓ^{TE}, and $\ell \in [30, 5000]$ for C_ℓ^{EE}. To represent additional constraints coming from low-ℓ polarization (e.g., from the *Planck* High Frequency Instrument) that break the degeneracy between τ and A_s (Aghanim et al. 2016), we include a Gaussian prior on τ with width $\sigma(\tau) = 0.01$.

The nonlinearity of matter fluctuations affects the CMB power spectrum at small scales mainly through lensing. While the effect on the CMB lensing power spectrum from the large-scale structure bispectrum can be significant (Böhm et al. 2016), the corresponding changes in the *TT*, *EE*, and *TE* angular power spectra are negligible (Lewis & Pratten 2016). We therefore do not consider the modeling uncertainties from nonlinear lensing effects on the CMB power spectra in this work.

2.3. Modeling Large-scale Structure Surveys

LSS surveys utilize a variety of tracers in order to probe the growth of structure in the universe as a function of cosmic time, such as galaxies, quasars, and the Lyα forest. These measurements, in turn, enable strong constraints to be placed on both early- and late-universe parameters (Tegmark et al. 2004; Samushia et al. 2012; Alam et al. 2017).

In the linear regime, the matter power spectrum can be computed for a given cosmology using Boltzmann codes such as `CAMB` (Lewis et al. 2000) or `CLASS` (Blas et al. 2011). On smaller scales, where linear perturbation theory breaks down, one must resort to other methods. These may include *N*-body or hydrodynamical simulations, or else semi-analytic prescriptions, for example, ones based on the halo model of LSS (Peacock & Smith 2000; Seljak 2000; Cooray & Sheth 2002). However, these methods are not guaranteed to capture all the relevant physics. The presence of redshift-space distortions (RSDs), which render the power spectrum observed in redshift-space anisotropic, further complicates matters.

Because we aim to investigate the impact of systematic errors on constraints from LSS, and those are mainly due to modeling uncertainties at small scales, we parameterize the observed galaxy power spectrum in a way that allows us to generically encapsulate modifications to our fiducial power spectrum due to nonlinear effects. Following Seo & Eisenstein (2007), we write the redshift-space power spectrum of tracer X as

$$P_{\rm obs}(k, \mu, z) = b_X^2(z)\left(1 + \frac{f(z)}{b_X(k, z)}\mu^2\right)^2 \times P_m(k, z)\exp\left[-\frac{k^2\mu^2\sigma_v^2}{H_0^2}\right]M_{\rm nl}(k, z), \quad (7)$$

where $P_m(k, z)$ is the matter power spectrum from `CAMB` with nonlinear corrections from `HMcode` (Mead et al. 2015), μ is the cosine of the angle between the line connecting galaxy pairs and the line of sight and $f(z) = d\ln D/d\ln a$ is the logarithmic derivative of the linear growth factor. The exponential term, featuring the velocity dispersion σ_v, models the power suppression along the line of sight at small scales due to RSDs (the so-called Figures-of-God effect). Here σ_v is calculated using the virial scaling relation from Evrard et al. (2008), evaluated at the characteristic mass of collapsed halos (M_*). We find that the effect only has a minor impact, slightly increasing the forecasted errors at $k_{\rm max} > 1\,h\,{\rm Mpc}^{-1}$. The impact of baryons and other effects on nonlinear scales (henceforth *nonlinear effects*) are accounted for by the as-yet undefined function $M_{\rm nl}(k, z)$. The term b_X^2 describes the linear galaxy bias for galaxy population X, which we define to have the redshift dependence of $b^2(z) = b_0^2(1 + z)$. We marginalize over the amplitude b_0 when determining cosmological parameter constraints, and absorb any scale-dependent bias effects into $M_{\rm nl}(k, z)$.

We now turn to the "nonlinear" function $M_{\rm nl}(k, z)$. We consider three treatments, in order of increasing complexity:

1. *No Nuisance model:* The simplest case is the trivial one where the nonlinear power is assumed to be modeled perfectly by the modified halo model prescription in `HMCode` and there is no scale-dependent bias. This corresponds to $M_{\rm nl}(k, z) = 1$, with no additional nuisance parameters. We refer to this as the No Nuisance model.
2. *Mead model:* The next model for $M_{\rm nl}(k, z)$ is the one presented by Mead et al. (2015), in which the modifications to nonlinear power due to baryonic feedback effects are parameterized using two parameters [A_b and η_0] (*Mead parameters*). In this case,
$$M_{\rm nl}(k, z) = \frac{P_{\rm Mead}(k, z, A_b, \eta_0)}{P_{\rm Mead,DMonly}(k, z)}, \quad (8)$$
where "DMonly" refers to the default Mead parameter values of $A_b = 3.13$ and $\eta_0 = 0.6044$.
3. *Many Free Parameter (MFP) model:* The final model for the nonlinearities is a much more agnostic prescription similar to Bielefeld et al. (2015), in which $M_{\rm nl}(k, z)$ is allowed to float freely in bins of wavenumber k and smoothly, as a low-order power law, in redshift. Since at low k the power spectrum is well determined theoretically, we allow $M_{\rm nl}(k, z)$ to vary only for k at the quasi-linear regime and above, setting it to unity at large scales.

   We therefore have
$$M_{\rm nl}(k, z) = \begin{cases}(1 + c_{1,k}z + c_{2,k}z^2)B_k & \text{if } k > 0.1\\ 1 & \text{if } k \leqslant 0.1\end{cases}, \quad (9)$$
where k has units $h\,{\rm Mpc}^{-1}$, and B_k, $c_{1,k}$, and $c_{2,k}$ are free parameters. One set of $\{B_k, c_{1,k}, c_{2,k}\}$ is specified in each wavenumber bin of width $\Delta\ln k = 0.05\,h\,{\rm Mpc}^{-1}$. This bin width is fixed, so as the maximum wavenumber $k_{\rm max}$ is raised, the number of k bins increases, and consequently so does the number of nuisance parameters. The total number of nuisance parameters in $M_{\rm nl}(k, z)$ thus ranges from 0 to 279 as $k_{\rm max}$ is varied from 0.1 to $10\,h\,{\rm Mpc}^{-1}$, and hence we refer to this as the MFP model.

The covariance between the observed power spectrum at wavenumbers k_α and k_β is given as the sum of the "unconnected" part, which is diagonal in the two wavenumbers, and the connected contribution given by the full trispectrum:

$$[{\rm Cov}]_{k_\alpha,k_\beta} = \frac{8\pi^2[P_{\rm obs}(k_\alpha, \mu, z)]^2}{V_{\rm eff}(k_\alpha, \mu, z)k_\alpha^2\Delta k_\alpha}\delta_{k_\alpha,k_\beta} + T_{k_\alpha,k_\beta}. \quad (10)$$

The effective volume of the survey varies with redshift and is given by

$$V_{\rm eff}(k,\,\mu,\,z) = V(z)_{\rm survey}\left[\frac{n(z)P_{\rm obs}(k,\,\mu,\,z)}{1+n(z)P_{\rm obs}(k,\,\mu,\,z)}\right]^2, \quad (11)$$

where $n(z)$ is the galaxy number density of each redshift bin and $V(z)_{\rm survey}$ is the volume in $[h^{-1}{\rm Mpc}]^3$,

$$V(z)_{\rm survey} = \int_{z_{\rm min}}^{z_{\rm max}} \Omega_{\rm survey}\frac{r(z')^2}{H(z')}dz'. \quad (12)$$

Here, $r(z)$ is the comoving distance, $H(z)$ is the Hubble parameter, and $\Omega_{\rm survey}$ is the sky coverage of the survey in steradians. The term T_{k_α,k_β} is the contribution from the trispectrum due to the non-Gaussian nature of the matter field,

$$T_{k_\alpha,k_\beta} = \int_{k_\alpha}\frac{d^3\boldsymbol{k}_1}{4\pi k_\alpha^2\Delta k_\alpha}\int_{k_\beta}\frac{d^3\boldsymbol{k}_2}{4\pi k_\beta^2\Delta k_\beta}T(\boldsymbol{k}_1,\,-\boldsymbol{k}_1,\,\boldsymbol{k}_2,\,-\boldsymbol{k}_2). \quad (13)$$

We obtain T_{k_α,k_β} with the same calculation method described by Wu & Huterer (2013), who use the halo model to calculate the trispectrum, showing that it is dominated by the one-halo term. We refer the interested reader to that work for details.

In their spectral running constraint forecasts, Muñoz et al. (2017) consider a wide survey like the Dark Energy Spectroscopic Instrument (DESI; Aghamousa et al. 2016) as well as a deep and narrow survey similar to the *Wide Field Infrared Survey Telescope* (Spergel et al. 2015), finding that they improve constraints on the runnings by ∼20% and 30%, respectively, when added to data from a CMB-S4 experiment. Here we take a Euclid-like survey to be our fiducial survey, and we include a DESI-like survey for comparison.

Euclid. Euclid (Laureijs et al. 2011) is a proposed space-based LSS survey with large sky coverage and a deep redshift distribution, which should provide excellent constraints on the evolution of dark energy. We use the spectroscopic sample defined in Laureijs et al. (2011), assuming 15,000 deg^2 ($f_{\rm sky}\approx 0.36$) and a total of 50 million galaxies. We use the redshift bins given in Table 6 of Font-Ribera et al. (2014), with thickness $\Delta z = 0.1$ in the range $z\in[0.6,\,2.1]$. We infer the effective number density in each bin as $n(z) = \bar{n}P_{0.14,0.6}(z)/P_{\rm obs}(k = 0.14\,h\ {\rm Mpc}^{-1},\,\mu = 0.6,\,z)$, where $\bar{n}P_{0.14,0.6}(z)$ is a quantity reported by Font-Ribera et al. (2014) and $P_{\rm obs}$ is calculated via Equation (7). The resulting $n(z)$ is shown in Figure 1.

DESI. The DESI (Aghamousa et al. 2016) is a Stage-IV ground-based spectroscopy experiment at the Mayall telescope in Arizona, which will target multiple tracer populations over 14,000 deg^2 ($f_{\rm sky}\approx 0.34$) with good signal-to-noise out to $z\lesssim 1.5$. Here too we adopt the distribution given in Font-Ribera et al. (2014), which combines projections for the populations of Luminous Red Galaxies, Emission Line Galaxies, and quasars (QSOs) into estimates of $\bar{n}P_{0.14,0.6}(z)$ in redshift bins of $\Delta z = 0.1$ in the range $z\in[0.1,\,1.9]$. We calculate an effective $n(z)$ for each bin in the same way as with the Euclid-like projections, and show them in Figure 1. We assume that the Euclid-like and DESI-like experiments do not overlap, and we combine their information by summing the Fisher matrices, as we describe below.

2.4. Forecasting

We forecast uncertainties of cosmological parameters as a function of $k_{\rm max}$ using a Fisher matrix analysis. The Fisher matrix formalism is an extremely simple and efficient method to estimate the errors on model parameters given a set of data (Tegmark et al. 1997; Albrecht et al. 2009). If one approximates the likelihood as a multi-variate Gaussian in the parameters around its peak, the resulting Hessian (matrix of second derivatives) can be used to calculate the forecasted uncertainties in the cosmological parameters. The better the actual constraints on the parameters are, the closer the likelihood function is to a Gaussian distribution, and the more accurate the Fisher matrix approximation is. To the extent that we are assuming powerful future surveys with small errors on most parameters, the Fisher matrix approximation should be excellent. More importantly, given that our MFP systematics case contains up to ∼300 parameters, a Fisher forecast is the only reasonably straightforward way to estimate the errors.

Under the assumption of Gaussian perturbations and Gaussian noise, the Fisher Matrix for CMB temperature and polarization anisotropies (Seljak 1997; Zaldarriaga & Seljak 1997; Eisenstein et al. 1999) can be written as

$$F_{ij}^{\rm CMB} = \sum_\ell A_{\ell,i}({\rm Cov}_\ell)^{-1}[A_{\ell,j}]^T, \quad (14)$$

where

$$A_{\ell,i} = \left(\frac{\partial C_\ell^{TT}}{\partial p_i},\,\frac{\partial C_\ell^{EE}}{\partial p_i},\,\frac{\partial C_\ell^{TE}}{\partial p_i}\right) \quad (15)$$

and the covariance is given by Equation (3). The Fisher matrix for the observed LSS power spectrum is

$$F_{ij}^{\rm LSS} = \sum_z\sum_\mu d\mu\sum_{k_\alpha,k_\beta}\frac{\partial P(k_\alpha,\,\mu,\,z)}{\partial p_i}\times[{\rm Cov}^{-1}]_{k_\alpha,k_\beta}\frac{\partial P(k_\beta,\,\mu,\,z)}{\partial p_j}, \quad (16)$$

where the sums are over all bins in z, μ, and k, and p_i runs over the cosmological parameters $\{\Omega_b h^2,\,\Omega_c h^2,\,\tau,\,H_0,\,n_s,\,A_s,\,\alpha_s,\,\beta_s\}$ as well as the linear bias parameter b_0 and the nuisance parameters in every k-bin, $\{B_k,\,c_{1,k},\,c_{2,k}\}$. We define k bins logarithmically, with $\Delta\ln k = 0.05$ in the range $k_{\rm max}\in[0.1,\,10]\,h\ {\rm Mpc}^{-1}$, and bin μ in 11 evenly spaced bins from -1 to 1.

Forecasts for a combination of experiments can be calculated by summing their Fisher matrices, and a forecast for the lower bound on the error for a given parameter is given by the Cramer–Rao inequality

$$\sigma(p_i)\geqslant\begin{cases}\sqrt{(F^{-1})_{ii}} & \text{(marginalized)}\\ 1/\sqrt{F_{ii}} & \text{(unmarginalized)}.\end{cases}$$

3. Results

We now present the principal results. To give an idea of the approximate overall level of constraint on the cosmological parameters, we summarize the fiducial constraints for our CMB-S4 forecast on the spectral runnings: when fixing $\beta_s = 0$, we obtain marginalized error on the spectral running of $\sigma_\alpha = 3.0\times10^{-3}$. When allowing β_s to vary, we find

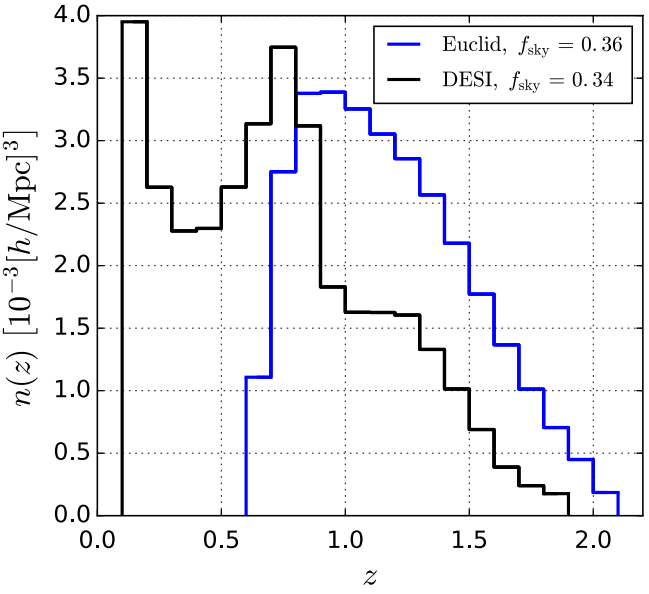

Figure 1. Galaxy number density $n(z)$ of Euclid and DESI in each redshift bin. The features in the DESI $n(z)$ are due to the fact that the sample is a combination of several populations of sources.

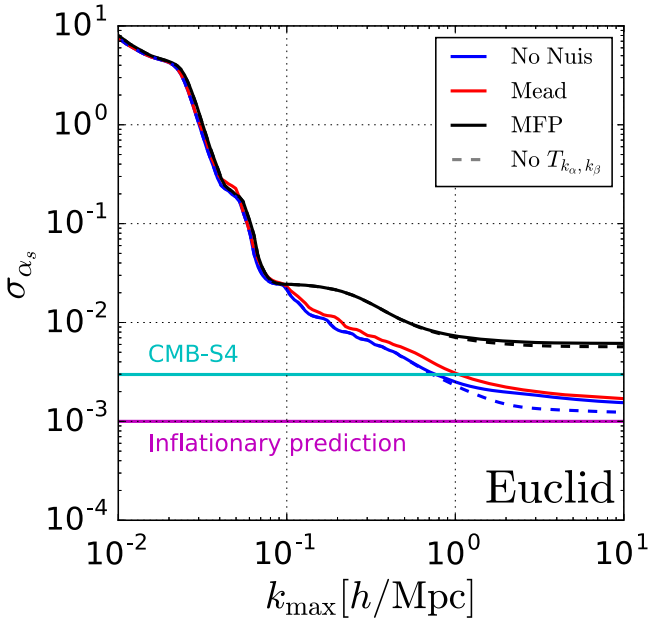

Figure 2. Error (1σ here and everywhere) in the spectral running α_s as a function of $k_{\rm max}$, evaluated for our fiducial Euclid-like survey, assuming $\beta_s = 0$. The legend shows our assumption about modeling of the systematics, while T_{k_α,k_β} refers to the inclusion of the trispectrum to the data covariance. Note that here and in subsequent plots, the value of the running denoted as the "Inflationary prediction" (purple horizontal line) is only approximate.

$\sigma_\alpha = 3.4 \times 10^{-3}$, $\sigma_\beta = 8.0 \times 10^{-3}$. (All constraints listed are the marginalized error, unless otherwise noted.) These constraints are similar to those of Muñoz et al. (2017), although slightly weaker because we do not include lensing information.

We now turn to the main goal of the paper: exploring whether and how adding information from LSS improves constraints on the spectral runnings. We first consider galaxy clustering alone, and then in conjunction with CMB-S4.

3.1. Galaxy Clustering

To see how information from LSS data at small scales impacts constraints on the first spectral running, we forecast the marginalized 1σ constraints on α_s as a function of $k_{\rm max}$. For the moment, we hold the second running β_s fixed at 0; we will let β_s vary further below, in Section 5.

Figure 2 shows the increase in constraining power when we include clustering information at small scales, comparing the performance of the No Nuisance (blue), Mead (red), and MFP models (black) for nonlinear effects. We also show constraints for the No Nuisance and MFP cases without the trispectrum contribution to the covariance (dashed), to demonstrate that its contribution to the error budget is minor (see Appendix A for a case where shot noise is suppressed and the trispectrum dominates the error budget).

In the No Nuisance case, that is, the forecast for constraints if no parameters need to be introduced to model nonlinear effects, we find a large gain in constraining power for high $k_{\rm max}$. This gain remains whether or not we include the trispectrum contributions to the power spectrum's covariance at small scales (solid and dashed curves, respectively). However, the overall gain with increasing $k_{\rm max}$, even in this no-systematics case, is not as significant as might be expected based on the behavior at linear scales, because the slope of the σ_α versus $k_{\rm max}$ curve changes at scales where nonlinearities become important, $k_{\rm max} \simeq 0.1\,h\,{\rm Mpc}^{-1}$. This flattening in $\sigma_\alpha(k_{\rm max})$ implies that, even in the optimistic no-systematics scenario and pushing out to $k_{\rm max} = 10\,h\,{\rm Mpc}^{-1}$, the Euclid constraint on the running would only be comparable to the expected inflationary signal, $\sigma_\alpha \simeq 10^{-3}$ and so be insufficient for a statistically significant detection of α of that size.

The red and black curves in Figure 2 show how these constraints respond to the addition of nuisance parameters intended to capture nonlinear effects, corresponding to the Mead and MFP models, respectively. The Mead model, which introduces only two new parameters, produces results similar to the No Nuisance case. In contrast, constraints become considerably weaker (e.g., by a factor of $\sim$5 at $k_{\rm max} = 10\,h\,{\rm Mpc}^{-1}$) for the MFP model, which captures nonlinear effects via an agnostic, piecewise-in-k $M_{\rm nl}(k, z)$ with MFPs (up to 279 for the highest $k_{\rm max}$). Thus, in this more conservative treatment of small-scale systematics, the gains from including high-k modes are rendered modest at best, particularly for $k_{\rm max} \gtrsim 1\,h\,{\rm Mpc}^{-1}$. We will show below in Section 4, however, that the MFP parameterization does protect the constraints against the systematic biases due to modeling uncertainties in the high-k power spectrum.

Clearly, in the comparison of forecasted constraints, the more gentle treatment of systematics (with fewer free parameters) in the Mead model produces more favorable results than the more agnostic MFP case. However, this comparison of statistics-only errors alone is not enough to answer the question of whether a given treatment of systematics is sufficient for an analysis. Rather, modeling choices must be made by balancing the consideration of expected constraining power with the need for nuisance parameters to protect against biases to the best-fit cosmological parameters. Accordingly, we compare our three $M_{\rm nl}(k, z)$ treatments by studying their relative ability to protect against biases in Section 4.

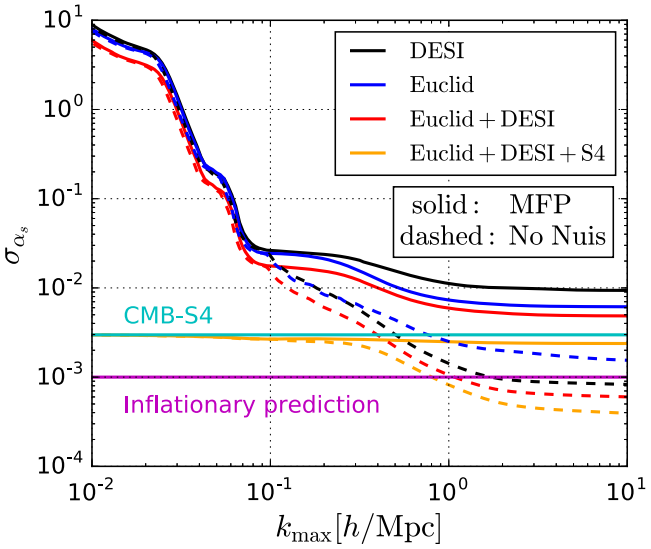

Figure 3. Marginalized constraints on α_s when combining information from different surveys (DESI-like, Euclid-like, CMB-S4, and also in combination). Solid curves include the MFP description of the systematic errors in galaxy surveys (see Equation (9), while the dashed curves do not. Results using the Mead parameterization are similar to the No Nuisance (No Nuis) case, and so we we omit them here for clarity.

3.2. Galaxy Clustering Plus CMB

The large lever arm provided by the combination of CMB and LSS allows for much tighter constraints on the running than using LSS data alone. We illustrate this in Figure 3, which gives the marginalized 1σ constraints on α_s for different $k_{\max}$ when combining LSS information from a Euclid-like and/or a DESI-like survey with that from a CMB-S4 experiment. We now show only forecasts that include the trispectrum contribution to the covariance, and use the comparison between the solid and dashed curves to compare the performance of the No Nuisance and MFP models, respectively. For clarity, we do not display the curves for the Mead model, which are similar to those for the No Nuisance case.

The curves for LSS data alone show results similar to those in Figure 2. We find that DESI and Euclid yield comparable errors in the running (with a ∼30% smaller error for Euclid), with their combination giving a slight improvement over Euclid alone.

As in the Euclid-only case, we see a 5–10× degradation in constraints if the MFP treatment of systematics is adopted compared to the No Nuisance case. We note that this degradation is greater for DESI (black) than for Euclid (blue).

Next we consider the effect of adding CMB-S4 information to the Euclid+DESI combination, which is shown in orange in Figure 3. When large and mildly nonlinear scales of the LSS ($k_{\max} \lesssim 0.5\ h\ \mathrm{Mpc}^{-1}$) are used, the CMB information dominates the (CMB+LSS) constraining power, and the combined error is essentially equivalent to that from CMB-S4 alone. At smaller scales, the LSS surveys help tighten constraints, but only in the No Nuisance case. In the MFP case, where many nuisance parameters are marginalized over, LSS data adds little constraining power on α_s compared to CMB-S4 data alone.

4. Systematic Biases in Model Parameters

The fact that there are significant modeling uncertainties associated with the theoretical prediction of galaxy clustering at small scales is our primary motivation for studying different choices of the $M_{\rm nl}(k, z)$ function to describe nonlinear effects. Any analysis will have to make simplifying choices for how to model the physics of nonlinear structure growth, baryonic effects, and scale-dependent galaxy bias. To the extent that those choices provide an incomplete description of the underlying physics there will be inaccuracies in the theoretical prediction for the observed galaxy power spectrum. Here we examine how these systematic errors—that is, residuals between the true and assumed power spectrum—impact parameter estimation for the spectral running.

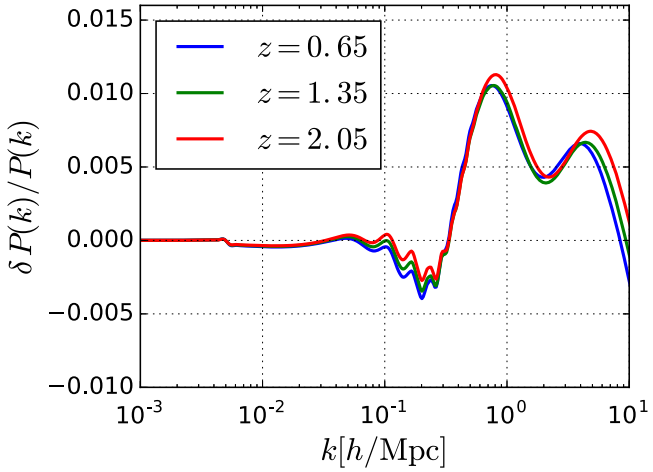

Figure 4. Relative difference between the nonlinear predictions from two popular fits: that of Takahashi et al. (2012) and of Mead et al. (2015) scaled so as to correspond to about 1% maximum difference at small scales. The quantity shown, $\delta P/P = 0.2(P_{\rm taka} - P_{\rm mead})/P_{\rm mead}$, is the fiducial model for the small-scale systematics that we employ in subsequent plots to gauge the protection offered by our systematics parameterizations.

In order to characterize this, we represent a typical form for the residuals due to systematic errors by taking the *difference* between two commonly used parameterizations of the matter power spectrum on small scales. Specifically, we subtract the nonlinear prescription by Takahashi et al. (2012) from that of Mead et al. (2015).[4] The power spectra generated with these two codes differ by up to ∼5%, roughly independent of redshift for the range considered. For the future surveys we consider, we optimistically assume that that theoretical advances will allow the small-scale power spectrum to be computed to an accuracy of about 1%. We therefore adopt a fifth of the Takahashi-Mead difference as our fiducial model for residual systematics, that is,

$$\delta P(k, \mu, z) = 0.2[P_{\rm Taka}(k, \mu, z) - P_{\rm Mead}(k, \mu, z)], \quad (17)$$

which we show in Figure 4 as a fraction of our fiducial power spectrum.

We use the Fisher matrix formalism to predict the bias that the residuals in Equation (17) will produce in cosmological parameters (Knox et al. 1998; Huterer 2002). In the limit where changes to best-fit parameters can be expanded linearly in small changes to the observations, the bias in parameter p_i can be

[4] We take the default parameter values of $A_{\rm bary}$ and η_0 corresponding to the DMONLY case in `HMcode` as of 2018 February, which includes the updates of Mead et al. (2016).

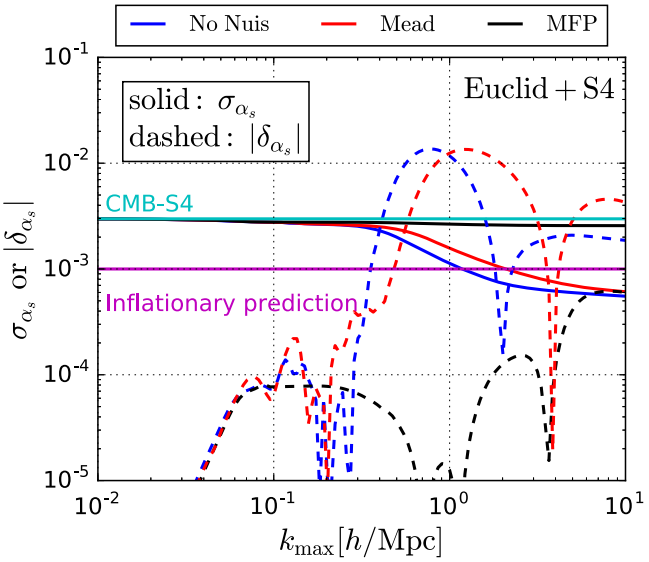

Figure 5. 1σ statistical errors (solid curves) and bias (dashed) in the first spectral running, as a function of $k_{\rm max}$. We adopt the Euclid+CMB-S4 combination of surveys. The legend on top denotes three alternate assumptions about the systematic error modeling: none (blue), Mead (red), and MFP (black).

written as

$$\delta p_i \approx \sum_j (F^{-1})_{ij} G_j, \tag{18}$$

where

$$G_j = \sum_{z,\mu,k_\alpha,k_\beta} d\mu \frac{\partial P(k_\alpha, \mu, z)}{\partial p_j} [{\rm Cov}^{-1}]_{k_\alpha,k_\beta} \delta P(k_\beta, \mu, z),$$

and Cov is the same covariance matrix defined in Equation (10). This formula is only accurate when the biases are small compared to the forecasted errors—that is, $|\delta p_i| \ll \sigma_{p_i} = \sqrt{(F^{-1})_{ii}}$—so we use it to determine the approximate threshold at which the bias on p_i becomes unacceptably large.

We plot both the bias $|\delta_{\alpha_s}|$ (dashed) and marginalized uncertainty σ_{α_s} (solid) for Euclid+CMB-S4 constraints on α_s in Figure 5. The value of $k_{\rm max}$ where the bias and uncertainty become comparable tells us roughly the smallest scales that can be included in an analysis without the systematic effects in δP adversely biasing the results for α. We see that though the MFP nuisance parameter prescription (black) has weaker constraints than the No Nuisance and Mead cases, it also is significantly better at protecting against bias. That is to say, on all $k_{\rm max}$ scales we examined, the bias in α for the MFP case is well below its statistical uncertainty. In contrast, the No Nuisance and Mead prescriptions have $\delta_{\alpha_s} \approx \sigma_{\alpha_s}$ at $k_{\rm max} \approx 0.4\,h$ Mpc^{-1} and $k_{\rm max} \approx 0.6\,h$ Mpc^{-1} respectively. Comparing the value for σ_{α_s} at these $k_{\rm max}$ values, we see that if we restrict ourselves to scales with $\delta_{\alpha_s} < \sigma_{\alpha_s}$, the improvement from adding high-k LSS data is marginal for all three $M_{\rm nl}(k, z)$ treatments.

To confirm that these results are robust against changes to the shape of our residual function $\delta P(k, z)$, we compared the same bias projections for a variety of other $\delta P_{i,j}(k, z) \propto P_i(k, z) - P_j(k, z)$, where $i, j \in$ (Mead (Mead et al. 2015), Takahashi (Takahashi et al. 2012), Bird (Bird et al. 2012), Peacock,[5] Halo model (Peacock & Smith 2000)) runs over a subset of possible prescriptions for the nonlinear matter power spectrum in CAMB. We normalized these so that the relative difference $\delta P_{i,j}(k, z)/P_{\rm Mead}$ had the same rms as our fiducial case[6] (see Appendix B). Thus the fiducial $\delta P(k, \mu, z)$ given in Equation (17) and the magnitude of resulting biases derived therefrom should be fairly representative of possible errors in modeling $P(k, z)$, while also aligning with the oft-quoted baseline assumption that uncertainties have to be controlled to 1% or better in order to not degrade the accuracy of future cosmological measurements of dark energy (e.g., Huterer & Takada 2005).

5. Constraining the Second Running: ΛCDM + α_s + β_s

We now expand the cosmological parameter space to include the second running β_s—that is, we extend our expansion of the spectral index to second order in $\ln k$. This is a parameter for which constraints from LSS data have the potential to be particularly interesting. Recent *Planck* results have suggested a positive second running β_s at nearly 2σ confidence which, if it persists, will help to discriminate between inflationary models (Cabass et al. 2016; Escudero et al. 2016). Additionally, as mentioned in Section 1, the current best-fit of $\beta_s = 0.025 \pm 0.013$ has important implications for physics of the late universe, as it makes PBHs a viable dark matter candidate (albeit with the requirement of a negative third-order running to avoid overproduction; Carr et al. 2016).

The left panel of Figure 6 shows that, when β_s is allowed to vary, combined constraints from CMB-S4 and LSS are no longer able to reach the inflationary prediction for α_s at any $k_{\rm max} < 10\,h$ Mpc^{-1}, even when the nonlinear $P(k, z)$ is modeled perfectly and with no nuisance parameters (solid blue curve). On the other hand, the right panel of Figure 6 shows that β_s itself benefits greatly from the addition of the LSS data. While CMB-S4 is expected to improve constraints on β_s by a factor of $\sim$4 over current levels, our results indicate that LSS data in the nonlinear regime from Euclid or DESI has the potential to improve this significantly up to $k_{\rm max} \sim 2\,h$ Mpc^{-1}, at which point shot-noise limits the information that can be gained.

We next consider the systematic biases in β_s using the same prescription as that in Section 4. Using our fiducial model for power spectrum residuals due to unaccounted-for systematics (Equation (17)), Figure 6 shows that, without introducing undue bias, adding data from a Euclid-like survey can improve constraints on β_s by a factor of 3–4 compared to the CMB-S4 only case.[7] While still an order of magnitude too large to reach β_s predicted by standard single-field slow-roll inflation, this level of precision is in the regime necessary to test for models relevant for PBH formation (Carr et al. 2016; Muñoz et al. 2017; Kohri & Terada 2018).

[5] http://www.roe.ac.uk/~jap/haloes

[6] For $k > 0.005\,h$ Mpc^{-1}, corresponding to the minimum k for which CAMB calculates nonlinear modifications to the power spectrum.

[7] This was the one case where our fiducial $\delta P(k, \mu, z)$ differed somewhat in its bias forecast from the ensemble of other $\delta P(k, \mu, z)$ tested, with $\delta_\beta/\sigma_\beta = 1$ occurring at $k_{\rm max} \approx 0.5$ and $0.7\,h$ Mpc^{-1} for the No Nuisance and Mead models, respectively ($\sim$4$\times$ improvement in σ_β), compared to $k_{\rm max} \approx 0.2$ and $0.4\,h$ Mpc^{-1} for the typical $\delta P(k, \mu, z)$ ($\sim$3$\times$ improvement in σ_β). The results are still qualitatively similar, however.

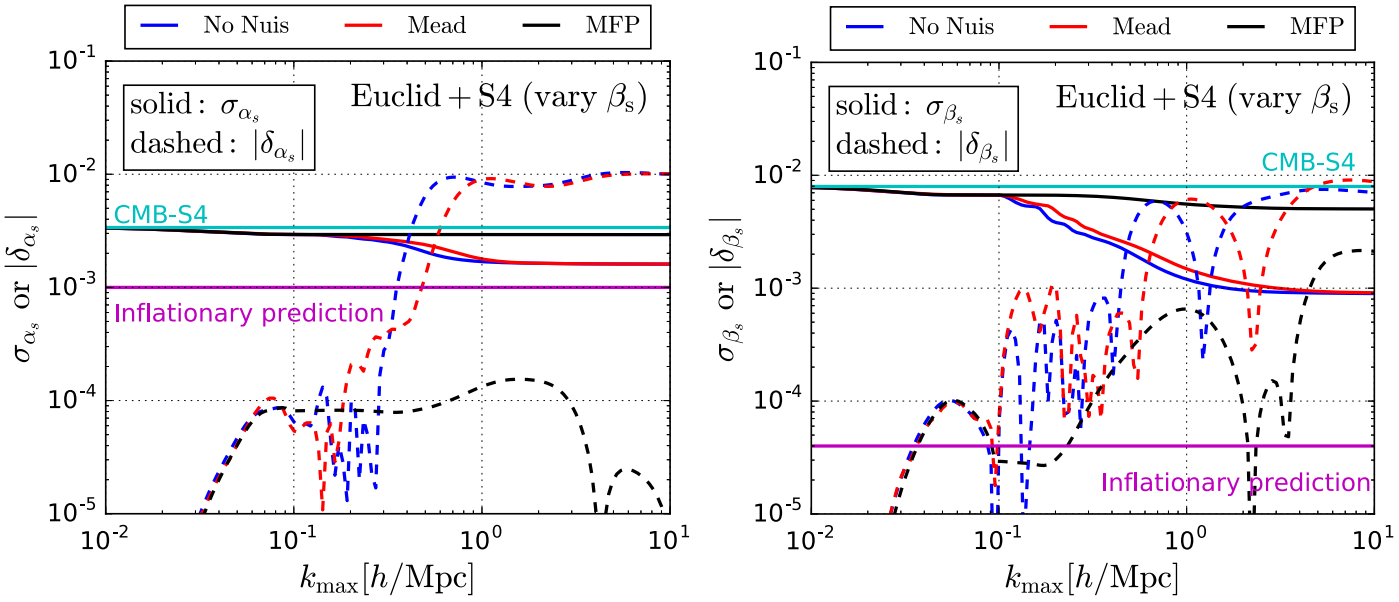

Figure 6. Similar to Figure 5, except now β_s is allowed to vary. The left panel shows the 1σ error and parameter bias in α_s as a function of $k_{\rm max}$, while the right panel shows the same for β_s. The curves have the same meaning as those in Figure 5.

6. Conclusions

In this work, we have investigated how small-scale information from LSS surveys can improve constraints on the first [α_s] and second [β_s] runnings of the scalar spectral index [n_s]. Previous analyses have been limited to the linear regime where the matter power spectrum is accurately described by theory, but the possibility of extending analyses to nonlinear regimes in the future is attractive. There are two reasons for this. First, there are many more modes at small scales and hence statistical errors from cosmic variance are greatly reduced. Second, accessing high k values provides a longer lever arm when combined with CMB constraints, which increases the sensitivity to variations in the spectral index and its runnings.

Attempts to include small-scale information are limited by challenges associated with theoretical modeling of the nonlinear power spectrum. Nonlinear clustering of dark matter, baryonic effects, and scale-dependent galaxy bias all contribute to modeling uncertainties on small scales. Therefore, it is critical to not only calibrate models for these effects as accurately as possible, but also to carefully characterize how analyses' cosmological results are affected by residual errors in predictions for small-scale power.

Motivated by these considerations, we compare forecasted constraints for spectral runnings from a few different parameterizations intended to capture the effects of systematics in the nonlinear regime. Specifically, we study cases where small scales are modeled using the fiducial halo model code (No Nuisance case), the parameterization from Mead et al. (2016), which introduces two nuisance parameters (Mead case), and an agnostic treatment adapted from Bielefeld et al. (2015) with up to a few hundred parameters, depending on $k_{\rm max}$ (Many Free Parameters, or MFP case).

We first study the forecasts for statistical errors on the first spectral running α_s for future LSS surveys like Euclid and DESI alone, as well as in combination with CMB-S4. We find that in the No Nuisance and Mead cases, the constraints from LSS surveys tighten substantially as $k_{\rm max}$ is raised to include nonlinear scales. The MFP case also shows improvement, but with a flatter dependence on $k_{\rm max}$ and weaker constraints overall. It is also at nonlinear scales where constraints using LSS and CMB data begin to improve α_s constraints compared to CMB-S4 data alone. The tightest constraints come from the Euclid+DESI+CMB-S4 combination, for which our No Nuisance forecasts for statistical errors reach a value of about a third of the α_s predicted by single-field slow-roll inflation at $k_{\rm max} \gtrsim 3\ h\ {\rm Mpc}^{-1}$. This could be precise enough to achieve a $\sim 3\sigma$ detection. These results become less promising, however, when we investigate the extent to which mismodeling of the nonlinear power spectrum biases cosmological parameter estimation. Using the difference between two commonly used nonlinear prescriptions as an example of expected modeling uncertainties, we determine the highest $k_{\rm max}$ we can use in an analysis before the resulting systematic bias in α_s becomes comparable to its statistical errors.

We find that for 1% errors in the power spectrum, in the No Nuisance case both α_s and β_s remain unbiased (i.e., bias is smaller than the 1σ statistical error) up to $k_{\rm max} \approx 0.3$–$0.4\ h\ {\rm Mpc}^{-1}$. Including these smaller scales results in significant improvements in σ_β, but only marginal improvements in σ_α. Adopting the Mead parameterization of the systematics leads to very similar results, indicating that the two free parameters from Mead et al. (2015), motivated to account for baryonic feedback, are not sufficient to offer protection against the 1%-level residual small-scale systematics in the power spectrum we might expect to encounter. In contrast, for the MFP parameterization α_s and β_s are unbiased for all $k_{\rm max}$ studied, but the statistical error on the runnings in the CMB +LSS scenarios is only marginally better than that of CMB-S4 alone.

Our level of optimism regarding future measurements of the spectral runnings using LSS data is therefore mixed. The values of α_s and β_s predicted by standard, single-field slow-roll models of inflation seem out of reach even when CMB-S4 information is combined with that of most powerful future LSS surveys once the small-scale systematics in the galaxy surveys are taken into account. On the other hand, larger values of

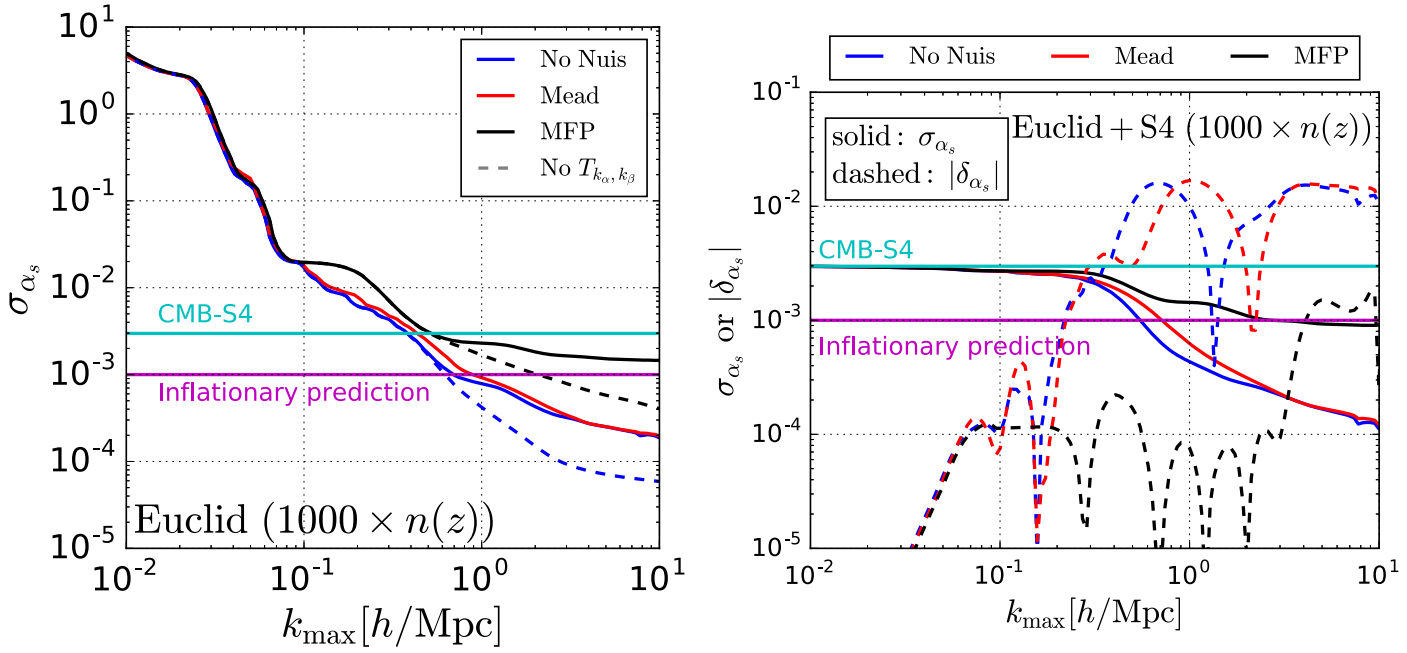

Figure 7. Constraints on the spectral running α_s for a hypothetical survey with $n(z) \rightarrow 1000 \times [n(z)_{\mathrm{Euclid}}]$ alone (left, compare to Figure 2) and with a CMB-S4 experiment (right, compare to Figure 5). While the LSS constraints improve with the increased number density, the trispectrum still limits the information that can be gained from nonlinear scales of $k \gtrsim 0.6\,h$ Mpc^{-1} (left, dashed vs. solid). If $P(k, z)$ is mismodeled, then only the MFP prescription (black) improves constraints over CMB-S4 before significantly biasing the results.

spectral runnings predicted by other classes of inflationary models, as well as those motivated by other physics (e.g., PBHs) are within reach, and should be testable with the next generation of surveys.

X.L. is supported by China Scholarship Council, National Key R&D Program of China No. 2017YFA0402600, the National Basic Science Program (Project 973) of China under Grant No. 2014CB845800, the National Natural Science Foundation of China under grant Nos. 11503001, 11633001, and 11373014, the Strategic Priority Research Program of the Chinese Academy of Sciences, grant No. XDB23000000, the Interdiscipline Research Funds of Beijing Normal University, and the Opening Project of Key Laboratory of Computational Astrophysics, National Astronomical Observatories, Chinese Academy of Sciences. D.H. and N.W. have been supported by DOE under contract DE-FG02-95ER40899. D.H. and S.A. have been supported by NASA under contract 14-ATP14-0005. J.M. has been supported by the Rackham Graduate School through a Predoctoral Fellowship.

Appendix A
Increasing the Number Density $n(z)$

As shown in Figures 2 and 5, a Euclid-like survey will be unable to constrain the spectral running to $\sigma_\alpha < 10^{-3}$, which would be necessary to be able to detect the value predicted by single-field, slow-roll inflation. To better understand the limiting factors of these forecasted constraints, we consider constraints for a survey similar to the Euclid-like one studied above, but with the number density increased dramatically to $n(z) \rightarrow 1000 \times n(z)$. We show forecasts for its statistical errors and systematic biases in Figure 7. We find that for this high-source-density survey, the LSS information tightens constraints at lower $k_{\max}$, reaching $\sigma_\alpha \lesssim 10^{-3}$ at $k_{\max} \approx \{0.5, 0.7, 2\}\,h$ Mpc^{-1} for the no nuisance, Mead, and MFP models, respectively. We also find that the increased density makes parameter estimation for α_s more sensitive to systematic biases: if $P(k)$ is mismodeled, then only the MFP model improves constraints over CMB-S4 before introducing unacceptable levels of bias.

This hypothetical $1000 \times n(z)$ survey is also useful to gauge the effect of the trispectrum-induced covariance on cosmological parameter constraints from modes in the strongly nonlinear regime. Unlike our main results in Figure 2, where the covariance term was shot-noise dominated at small scales, the trispectrum term becomes important when the number density is very high. The result, as can be seen in Figure 7, is that there is little improvement in σ_α—especially when combining with CMB-S4—from wavenumbers $k \gtrsim 2\,h$ Mpc^{-1}. Note that we have not included the additional "super-sample covariance" term (Takada & Hu 2013) that could further degrade the contribution from modes in the nonlinear regime.

Therefore, we conclude that, once the realistic systematics are accounted for, even a Euclid-like survey with an artificially high number density of sources is unable to reach the precision required to detect the spectral runnings predicted by single-field, slow-roll inflationary models.

Appendix B
Robustness of Results to Choice of $\delta P(k, \mu, z)$

As noted in Section 4, here we consider the robustness of our parameter bias results against changes to the shape of $\delta P(k, \mu, z)$. We do this by computing the differences between various prescriptions for the nonlinear power spectrum available in `CAMB`. Because we want to test sensitivity to the shape of $\delta P(k, \mu, z)$, we normalize each curve so that its rms over all z and $0.005 < k \leqslant 10\,h$ Mpc^{-1} is equal to that of our fiducial "takahashi-mead" $\delta P(k, \mu, z)$.

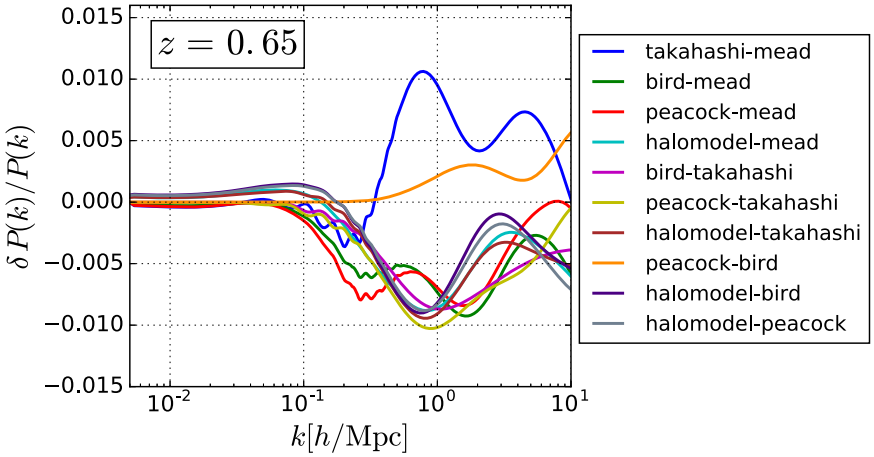

Figure 8. Other systematic shifts in $P(k)$ tested to verify that the results of Section 4 are robust to the choice of $\delta P(k)$. Note that because Equation (18) is linear in $\delta P(k)$ and we are interested in where $|\delta|/\sigma = 1$, the overall sign of $\delta P(k)$ is inconsequential.

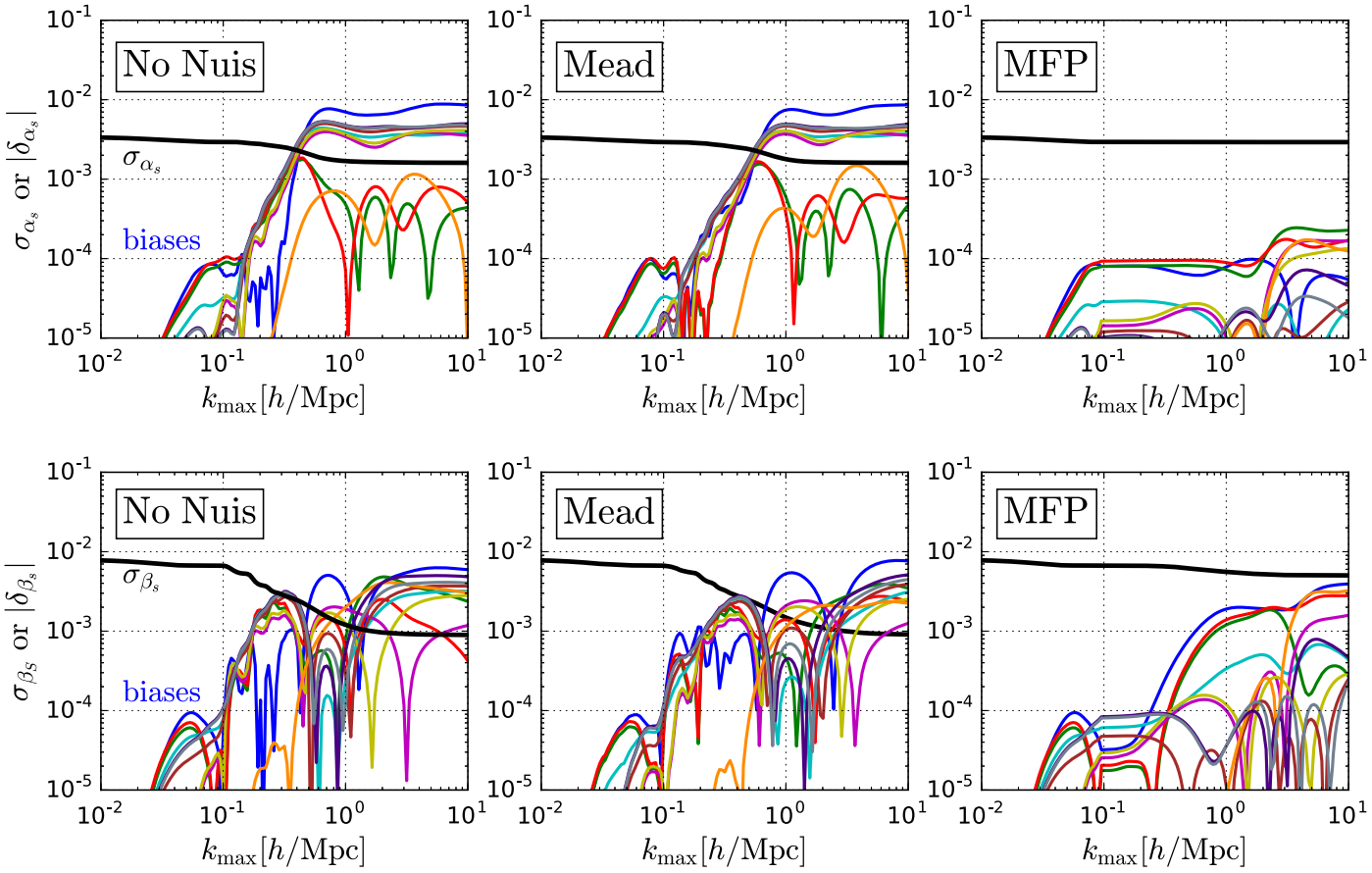

Figure 9. Parameter bias from different $\delta P(k, z)$ for $\Lambda\mathrm{CDM} + \alpha_s + \beta_s$ using Euclid + CMB-S4 for α_s (top) and β_s (bottom). The 1σ uncertainty is in black and columns correspond to different nonlinear prescriptions from Section 2.

Figure 8 shows the resulting ensemble of $\delta P(k, \mu, z)$ considered, for the shallowest redshift bin, $z = 0.65$. When looking at this figure, there are a couple of things worth noting. First, because we are primarily interested in how constraints on the runnings become biased as we push to higher scales, i.e., $k_{\max}$ at which $|\delta_{p_i}|/\sigma_{p_i} = 1$, the results are insensitive to the sign of $\delta P(k, \mu, z)$. Second, the relatively small magnitude of the bird−peacock (orange) curve is due to its large magnitude at higher redshifts compared to the other curves. Thus the low-z range shown contributes less to its normalized rms than it does for the other curves.

The parameter biases in α_s and β_s resulting from these $\delta P(k, \mu, z)$ curves are shown in Figure 9 for the combined analysis of Euclid and CMB-S4. These biases are analogous to those shown in Figure 6. Though there is certainly variation in the shape of the curves, we see that the results for $\delta_{\alpha_s}(k_{\max})$ and $\delta_{\beta_s}(k_{\max})$ for our fiducial $\delta P(k, \mu, z)$ (blue solid curves) are fairly typical. Therefore, we conclude that our fiducial choice

of the uncorrected bias in $P(k, z)$ at small scales, given in Equation (17), is fairly typical of such choices.

References

Abazajian, K. N., Adshead, P., Ahmed, Z., et al. 2016, arXiv:1610.02743
Ade, P. A. R., Aghanim, N., Arnaud, M., et al. (Planck) 2016a, A&A, 594, A20
Ade, P. A. R., Aghanim, N., Arnaud, M., et al. (Planck) 2016b, A&A, 594, A13
Aghamousa, A., Aguilar, J., Ahlen, S., et al. 2016, arXiv:1611.00036
Aghanim, N., Ashdown, M., Aumont, J., et al. (Planck) 2016, A&A, 596, A107
Alam, S., Ata, M., Bailey, S., et al. 2017, MNRAS, 470, 2617
Albrecht, A., Amendola, L., Bernstein, G., et al. 2009, arXiv:0901.0721
Albrecht, A., & Steinhardt, P. J. 1982, PhRvL, 48, 1220
Amendola, L., Appleby, S., Bacon, D., et al. 2013, LRR, 16, 6
Bardeen, J. M., Steinhardt, P. J., & Turner, M. S. 1983, PhRvD, 28, 679
Basse, T., Hamann, J., Hannestad, S., & Wong, Y. Y. Y. 2015, JCAP, 1506, 042
Bernardeau, F., Colombi, S., Gaztanaga, E., & Scoccimarro, R. 2002, PhR, 367, 1
Bielefeld, J., Huterer, D., & Linder, E. V. 2015, JCAP, 2015, 023
Bird, S., Viel, M., & Haehnelt, M. G. 2012, MNRAS, 420, 2551
Blas, D., Lesgourgues, J., & Tram, T. 2011, JCAP, 2011, 034
Böhm, V., Schmittfull, M., & Sherwin, B. D. 2016, PhRvD, 94, 043519
Cabass, G., Di Valentino, E., Melchiorri, A., Pajer, E., & Silk, J. 2016, PhRvD, 94, 023523
Carr, B., Kuhnel, F., & Sandstad, M. 2016, PhRvD, 94, 083504
Chisari, N. E., Richardson, M. L. A., Devriendt, J., et al. 2018, arXiv:1801.08559
Cooray, A., & Sheth, R. K. 2002, PhR, 372, 1
Czerny, M., Kobayashi, T., & Takahashi, F. 2014, PhLB, 735, 176
Dodelson, S. 2003, in AIP Conf. Proc. 689, Neutrinos, Flavor Physics, and Precision Cosmology (Melville, NY: AIP), 184
Drees, M., & Erfani, E. 2012, JCAP, 1201, 035
Easther, R., & Peiris, H. 2006, JCAP, 0609, 010
Eisenstein, D. J., Hu, W., & Tegmark, M. 1999, ApJ, 518, 2
Escudero, M., Ramírez, H., Boubekeur, L., Giusarma, E., & Mena, O. 2016, JCAP, 1602, 020
Evrard, A. E., Bialek, J., Busha, M., et al. 2008, ApJ, 672, 122
Font-Ribera, A., McDonald, P., Mostek, N., et al. 2014, JCAP, 2014, 023
Garcia-Bellido, J., & Roest, D. 2014, PhRvD, 89, 103527
Guth, A. H. 1981, PhRvD, 23, 347
Heitmann, K., Higdon, D., White, M., et al. 2009, ApJ, 705, 156
Heitmann, K., White, M., Wagner, C., Habib, S., & Higdon, D. 2010, ApJ, 715, 104
Huang, Z., Verde, L., & Vernizzi, F. 2012, JCAP, 1204, 005
Huterer, D. 2002, PhRvD, 65, 063001
Huterer, D., & Takada, M. 2005, APh, 23, 369
Knox, L., Scoccimarro, R., & Dodelson, S. 1998, PhRvL, 81, 2004
Kobayashi, T., & Takahashi, F. 2011, JCAP, 1101, 026
Kohri, K., & Terada, T. 2018, arXiv:1802.06785
Kosowsky, A., & Turner, M. S. 1995, PhRvD, 52, R1739
Laureijs, R., Amiaux, J., Arduini, S., et al. 2011, arXiv:1110.3193
Lawrence, E., Heitmann, K., White, M., et al. 2010, ApJ, 713, 1322
Lewis, A., Challinor, A., & Lasenby, A. 2000, ApJ, 538, 473
Lewis, A., & Pratten, G. 2016, JCAP, 1612, 003
Linde, A. D. 1982, PhLB, 108, 389
Mead, A., Heymans, C., Lombriser, L., et al. 2016, MNRAS, 459, 1468
Mead, A., Peacock, J., Heymans, C., Joudaki, S., & Heavens, A. 2015, MNRAS, 454, 1958
Muñoz, J. B., Kovetz, E. D., Raccanelli, A., Kamionkowski, M., & Silk, J. 2017, JCAP, 2017, 032
Peacock, J. A., & Smith, R. E. 2000, MNRAS, 318, 1144
Rudd, D. H., Zentner, A. R., & Kravtsov, A. V. 2008, ApJ, 672, 19
Samushia, L., Percival, W. J., & Raccanelli, A. 2012, MNRAS, 420, 2102
Scoccimarro, R., Zaldarriaga, M., & Hui, L. 1999, ApJ, 527, 1
Seljak, U. 1997, ApJ, 482, 6
Seljak, U. 2000, MNRAS, 318, 203
Seo, H.-J., & Eisenstein, D. J. 2007, ApJ, 665, 14
Smith, R. E., Peacock, J. A., Jenkins, A., et al. 2003, MNRAS, 341, 1311
Spergel, D., Gehrels, N., Baltay, C., et al. 2015, arXiv:1503.03757
Takada, M., & Hu, W. 2013, PhRvD, 87, 123504
Takahashi, R., Sato, M., Nishimichi, T., Taruya, A., & Oguri, M. 2012, ApJ, 761, 152
Tegmark, M., Strauss, M. A., Blanton, M. R., et al. 2004, PhRvD, 69, 103501
Tegmark, M., Taylor, A. N., & Heavens, A. F. 1997, ApJ, 480, 22
van Daalen, M. P., Schaye, J., Booth, C. M., & Vecchia, C. D. 2011, MNRAS, 415, 3649
Vieira, J., Byrnes, C., & Lewis, A. 2018, JCAP, 1, 19
Wu, H.-Y., & Huterer, D. 2013, MNRAS, 434, 2556
Zaldarriaga, M., & Seljak, U. 1997, PhRvD, 55, 1830